Supporting Information for

Time-resolved Magnetic Field Effects distinguish Loose Ion Pairs from Exciplexes

Sabine Richert,[1] Arnulf Rosspeintner,[1] Stephan Landgraf,[2] Günter Grampp,[2] Eric Vauthey,[1] and Daniel Kattnig*,[2]

[1] *Department of Physical Chemistry, University of Geneva, 1211 Geneva 4, Switzerland.*

[2] *Institute of Physical and Theoretical Chemistry, Technische Universität Graz, Stremayrgasse 9, 8010 Graz, Austria.*

E-mail: daniel.kattnig@tugraz.at

Table of Contents

List of Figures

Experimental Details

Two independent experimental setups located in Graz and Geneva have been used to obtain the experimental results presented in this work. The obtained results can be combined to a unified picture demonstrating the robustness of the measured data.

Setup 1 (Geneva)

Chemicals. 9,10-dimethyl anthracene (Fluka, 97 %) was used as received. N,N-dimethylaniline (DMA, Aldrich, Reagent Plus® 99%) was distilled under reduced pressure and stored in the dark under argon atmosphere. Propyl acetate (PA, Alfa Aesar, 99%) and butyronitrile (BN, Fluka, purum $\geq$ 99.0%) were distilled prior to use.

Spectroscopy. Absorption spectra were recorded on a Cary 50 absorption spectrometer. Emission spectra were recorded on a Cary Eclipse fluorimeter. Nanosecond time-resolved emission decays in the absence and presence of a magnetic field were recorded using a home-built time-correlated single photon counting apparatus with a 395 nm laser diode (Picoquant, LDH-P-C-405) as excitation light source. The emission passing through a polarizer foil at magic angle with respect to the vertically polarized excitation was recorded. Appropriate filters were used allowing for the observation of either locally excited state (420 nm interference filter) or exciplex (600 nm long pass filter). A magnetic field of approx. 150 mT was applied using a set of permanent magnets. The emission was monitored at a geometrical angle of 30° with respect to optical excitation. All time traces were recorded in a 800 ns window at a repetition rate of 500 kHz using a delay generator (Stanford research systems). The absence of interferences of the magnetic field with the detection system was tested by comparing emission decays of the pure fluorophore in the absence and presence of a magnetic field. The samples with 0.05 M DMA were prepared in septa-sealed 10 mm fluorescence quartz cuvettes by adding corresponding amounts of DMA via Hamilton syringes to the already degassed fluorophore solutions. Subsequently the samples were deoxygenated by sparging with argon for approx. 15 minutes. Contamination of the exciplex time traces by residual locally excited state fluorescence was precluded by measuring a sample of the fluorophore without quencher with the longpass emission filter for the exciplex measurements in place.

Setup 2 (Graz)

Chemicals. The quencher DMA (99.5%, purified by redistillation) and the fluorophores pyrene (99%) and pyrene-d_{10} (98 atom % D) were purchased from Aldrich and used as re-

ceived. 9,10-Dimethyl anthracene (Aldrich, 99%) was recrystallized from ethanol. The solvents butyronitrile (Aldrich, 99%) and propyl acetate (Aldrich, 99.5%) were purified by distillation prior to use. All samples were prepared and stored under argon atmosphere. Additionally, oxygen was removed by bubbling solvent-saturated argon through the septa-sealed cuvettes for 20 minutes directly before every measurement.

Spectroscopy. Absorption spectra were recorded on a Shimadzu UV-3101-PC UV-VIS-NIR spectrophotometer. The sample fluorescence was measured on a thermostatted Jobin Yvon Fluoromax-2 spectrofluorimeter. The temperature for fluorescence measurements was held constant at $\theta = 22^\circ$ C with the help of a Haake F3 thermostat. The setup used to record the time-resolved exciplex traces is depicted in Figure S1. In order to record the luminescence decay as a function of time, the light source was driven by a pulser (Picoquant, PDL-800B) with a repetition rate adjustable from 40 to 2.5 MHz. The pulser also serves to generate the so-called SYNC signal being the start signal for the time-to-amplitude converter (TAC). As the signal is generated electronically, no constant fraction discriminator (CFD) has been used in the SYNC channel. The light source used for excitation of the sample was a 374 nm laser diode (Picoquant, LDH series, Pulse FWHM 60 ps).[1] Right in front of the light source, an excitation filter **3** (UG1) was placed. The intensity of the light source was adjusted via an iris **2**. A cone-shaped reflecting pipe **4** was used to collect the light and guide it directly into the cuvette **6**, where the sample is excited. The sample itself is contained in a thermostattable sample holder which is located between the pole shoes of an electromagnet. The radiation emitted by the sample is transported to the detector with the help of a liquid light guide **10** (Lumatec, series 300). A high voltage **12** driven photomultiplier tube (PMT, Hamamatsu, R5600-U04) in combination with a non-fluorescing emission filter LP 550 **11** is used to detect the optical signal. Its output delivers the stop pulse for the TAC (Ortec, model 567). As the amplitude of the PMT output signal is only in the range of some 20 mV, a pre-amplifier **13** (Ortec, VT120) is used before the signal is transferred to the constant fraction discriminator (CFD). At the TAC the information from the two signal paths is evaluated and transferred to the multi channel analyzer (Ortec, EASY-MCA) where a histogram of single photon events is generated. To study the influence of a magnetic field on the reaction, a magnet power supply **1** in combination with the Helmholtz coils **7** and a DC offset **5** have been used to adjust the magnetic field strength. On the gaussmeter **9** the actual field value sensed by the hall probe **8** is read off.

[1] Also pyrene can be excited at this wavelength as only little excited state population is necessary. We take advantage of its low-intensity forbidden transition at this wavelength and thereby avoid direct excitation of the quencher DMA.

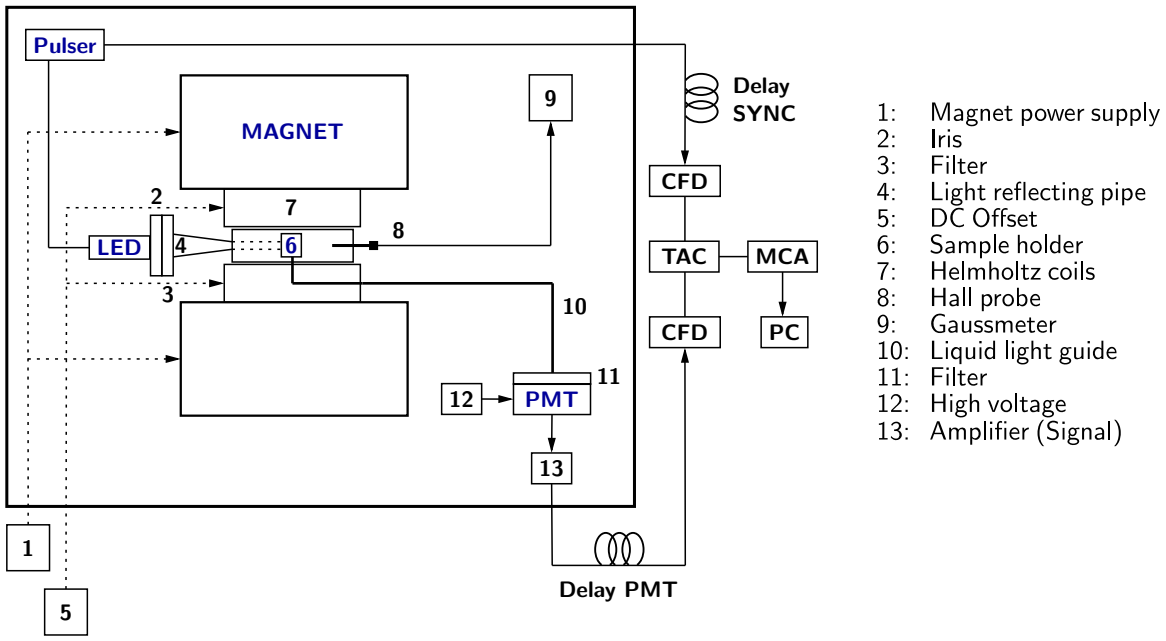

Figure S1: Scheme of the employed setup.

All MFE measurements have been performed at 295 K and at a repetition rate of 2.5 MHz. The permittivity of the solvent was adjusted making use of solvent mixtures composed of butyronitrile and propyl acetate. Light reflections produced at the light guide window facing the PMT were observed and could be reduced by optically coupling the light guide to the cuvette using some drops of glycerol (80%). For every sample, measurements at 0 and 500 G were carried out where the field was measured perpendicular to the excitation. The time traces were obtained by collecting single photon events during 600 s (realtime) at a start-to-stop ratio of about 40. The high-voltage settings and the light intensity (iris settings) remained equal during all measurements. Using 10^{-5} M 9,10-dimethyl anthracene, measurements at relative solvent permittivities of $\varepsilon_r = 15$ ($V_{PA} : V_{BN} = 1 : 1$), 20 ($V_{PA} : V_{BN} = 1 : 3.3$), and 25 (pure BN) have been performed. The pyrene (10^{-5} M) and pyrene-d_{10} (10^{-5} M) measurements have been carried out in pure butyronitrile which has a relative permittivity of 25 at 295 K. DMA at a concentration of 50 mM was used as the quencher in all cases.

In the setup used in Graz the earth magnetic field has been compensated in one direction whereas in the setup used in Geneva the earth magnetic field was not compensated. Note that, despite this fact, no differences in the experimental results are observed.

Calculation of the Singlet Probability

The singlet probability $p_S(t, B_0)$ is given by

$$p_S(t, B_0) = Tr\left[\hat{P}_S\,\hat{\rho}(t, B_0)\right] \tag{S1}$$

where $\hat{P}_S$ denotes the singlet projection operator, Tr is the trace operation, and the time-behavior of the spin density matrix $\hat{\rho}(t, B_0)$ is obtained from the Liouville-von-Neumann equation:

$$\frac{d\hat{\rho}}{dt} = -i\,\left[\hat{H}, \hat{\rho}\right] + \hat{\hat{K}}_{ex}\,\hat{\rho} \tag{S2}$$

with the initial density matrix given by:

$$\hat{\rho}(t = 0) = \frac{\hat{P}_S}{Tr(\hat{\rho})} \tag{S3}$$

In the low-viscosity approximation, the exchange interaction can be neglected, thus, the Hamiltonian $\hat{H}$ for a single radical i only contains contributions from the Zeeman interaction of the electron spins and the hyperfine interactions according to

$$\hat{H}_i = g_i \mu_B B\,\hat{S}_{i,z} + \sum_j a_{ij}\,\hat{S}_i \cdot \hat{I}_{ij} \tag{S4}$$

Since only moderate magnetic fields are employed, it is furthermore assumed that $g_{r1} = g_{r2} = 2.0023$. The influence of the exchange operator $\hat{\hat{K}}_{ex}$ accounting for degenerate electron exchange is then calculated from:

$$\hat{\hat{K}}_{ex}\,\hat{\rho} = \frac{1}{\tau_{ex}}\left[Tr_n(\hat{\rho}) \otimes \frac{\hat{1}}{N} - \hat{\rho}\right] \tag{S5}$$

In this work, the spin correlation tensor approach was used to calculate the singlet probability. This approach implies a reformulation of Eqs (S2,S3,S5) which allows a more efficient numerical treatment of the problem in Hilbert space. Details can be found in references [1–3]. Concerning the exchange rate $k_{ex} = \frac{1}{\tau_{ex}}$, a value of $\tau_{ex} = 8\,\text{ns}$ was used in all simulations [4].

Figure S2 shows the singlet probabilities calculated for the system 9,10-dimethyl anthracene/DMA in the zero and high field limits with and without electron self exchange taken into account. In Figure S3 the calculated singlet probabilities for pyrene-h_{10}/DMA and pyrene-d_{10}/DMA are shown as a function of time. Marked differences are observed when electron self exchange is not taken into account. Only when accounting for electron self exchange, the experimental data can be properly described.

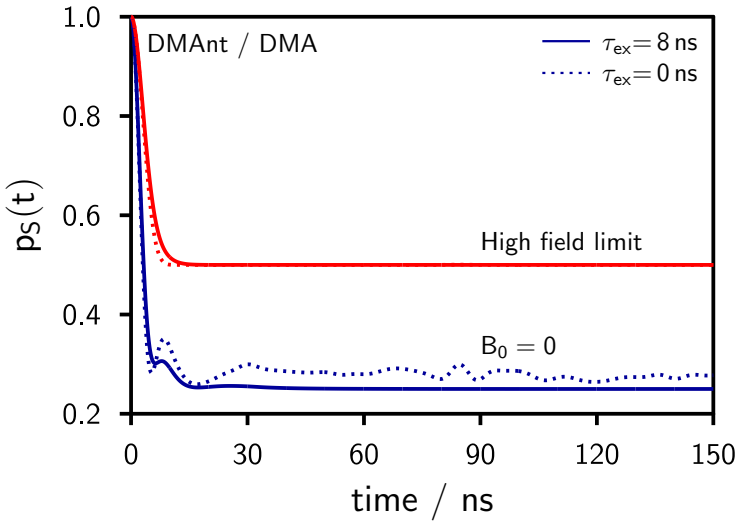

Figure S2: Calculated singlet probability as a function of time for 9,10-dimethyl anthracene/ DMA in the zero and high field limit. The dashed lines show the time behavior obtained when neglecting electron self exchange, whereas the solid lines represent the time-behavior for $\tau_{ex} = 8$ ns.

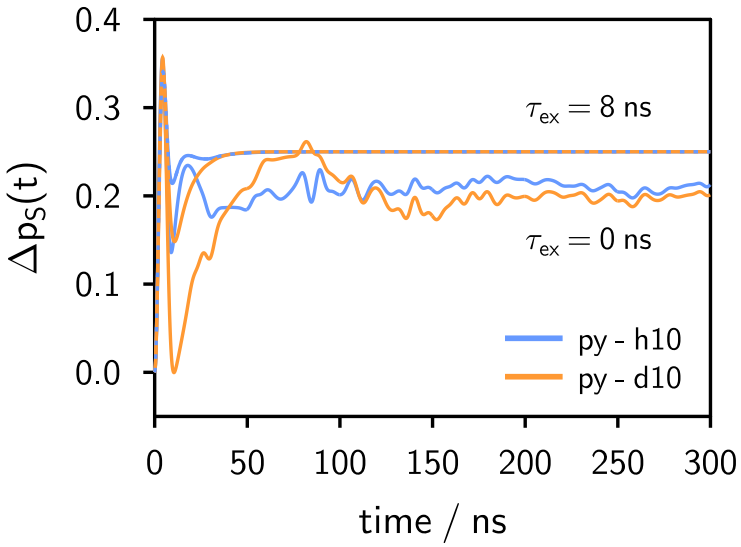

Figure S3: Calculated singlet probability $\Delta p_S = p_S(B_0) - p_S(0)$ as a function of time for pyrene-h_{10}/DMA and pyrene-d_{10}/DMA. The solid lines show the time behavior obtained when neglecting electron self exchange, whereas the dashed lines represent the time-behavior for $\tau_{ex} = 8$ ns.

Calculation of the Singlet Yield / Recombination

In this work a diffusion Green's function approach [5, 6] has been used to calculate the singlet yields from:

$$R(t, B_0 \mid r_I) = \int_0^t p_S(t, B_0)\, f(t \mid r_I)\, \exp\left(-\frac{t}{\tau_R}\right) \mathrm{d}t \tag{S6}$$

with $f(t \mid r_I)$ denoting the recombination flux, and τ_R the lifetime of the radical pair. The recombination flux is then defined as:

$$f(t \mid r_I) = k_a\, n(r_E, t \mid r_I) \tag{S7}$$

with the time-dependence of $n(r, t)$ given by:

$$\frac{\partial n(r,t)}{\partial t} = \frac{1}{r^2}\frac{\partial}{\partial r} D(r)\, r^2\, \exp(r/r_c)\, \frac{\partial}{\partial r} \exp(-r/r_c)\, n(r,t) \tag{S8}$$

where $r_c = \frac{e_0^2}{4\pi\,\varepsilon_0 \varepsilon_r\, k_B\, T}$ denotes the Onsager radius. The initial condition (for instantaneous RIP generation) is taken to be

$$n(r, t=0) = \delta(r - r_I)/4\pi\, r^2 \tag{S9}$$

and the system obeys the radiation boundary condition

$$\left(\frac{\partial n}{\partial r} + \frac{r_c}{r^2}\, n - \frac{k_a}{4\pi\, r_E^2\, D(r_E)}\, n\right)\Bigg|_{r=r_E} = 0 \tag{S10}$$

Additional Details on the Simulations Using Model 2

According to the above-listed formulas, the time evolution of the magnetic field effect depends on the following parameters:

- Diffusive motion: D, r_E, r_c, hydrodynamic hindrance
- Exciplex: τ_E, $\phi_{\mathrm{diss}} = k_d\, \tau_E$
- RIP: spin evolution, τ_R, r_I, ϕ_I, $k_a = K_A\, k_d$

At first glance, it might seem that the used model introduces many new freely variable parameters but, in fact, most of these listed variables are either known, or can be determined in independent experimental measurements and kept constant during the simulations.

The parameters describing the diffusive motion are known, τ_E can be determined experimentally, and also ϕ_{diss} was shown to be experimentally accessible from a plot of the exciplex lifetime τ_E as a function of the solvent permittivity ε_r. Spin evolution can also reliably be calculated, thus the only unknown parameters are in fact τ_R, r_I, ϕ_I, and $k_a = K_A\, k_d$. Only two of these four parameters, namely ϕ_I and $k_a = K_A\, k_d$, were found to have a pronounced effect on the result of the simulation (cf. Figure S4), while the influence of the radical ion pair lifetime τ_R and the distance where the ions are generated by distant electron transfer r_I is small (when kept in a reasonable range), so that these parameters can be kept fixed during the simulation.

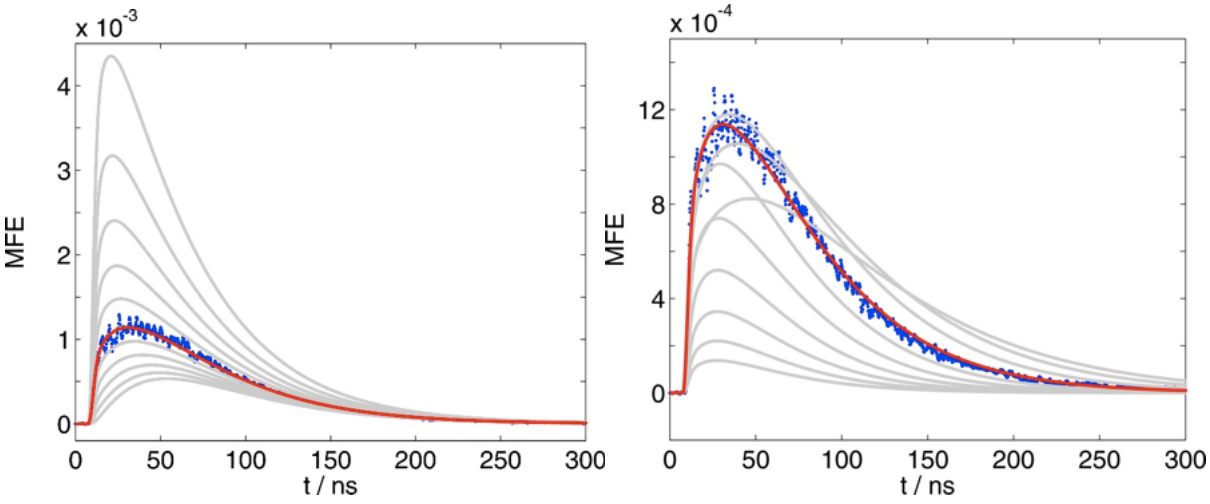

Figure S4: Influence of the fitting parameters ϕ_I (left) and K_A (right) on the time-resolved magnetic field effect. The experimental data can be reproduced with $\phi_I = 0.48$ and $K_A = 13\,\mathrm{M}^{-1}$. The magnetic field effect amounts to $\chi_E = 10.8\,\%$. When varying these two parameters (gray lines) the magnitude as well as the shape of the time-resolved magnetic field effect are strongly influenced.

The graph on the left hand side of Figure S4 shows the influence of the fitting parameter ϕ_I on the time-resolved magnetic field effect. It can be seen that the magnitude as well as the shape of the time-resolved MFE are considerably affected when varying ϕ_I (gray lines) and only for $\phi_I = 0.48$ the experimental data can be well reproduced. The time-resolved MFE also strongly depends on the fitting parameter K_A as becomes obvious from the graph on the right hand side of Figure S4. The best fit is obtained for $K_A = 13\,\mathrm{M}^{-1}$ and the magnetic field effect amounts to $\chi_E = 10.8\,\%$.

As already mentioned above, all other parameters, apart from ϕ_I and K_A, introduced in the framework of model 2, usually have only minor influence and can be kept fixed during the simulations. Typical values for the simulation parameters which have been used in this work are given in Table S1. Tables S2-S5 list the hyperfine coupling constants that have been used to calculate the spin evolution of the RIP.

Table S1: Simulation parameters used in this work. The values given apply to the system 9,10-dimethyl anthracence/DMA at $\varepsilon_r = 17$. See references [7, 8] for the calculation of the distant-dependent diffusion coefficient $D(r) = \gamma(r)\, D$.

Parameter	**Value**
r_E	6.8 Å
D	220 Å^2/ ns (Stokes-Einstein, stick)
$\gamma(r)$	Deutch-Felderhof
r_I	8.5 Å
ϕ_d	0.70
τ_R	100 ns

Table S2: Used hyperfine coupling constants for $DMA^{\bullet+}$. As no experimental values are available, the values have been calculated using Gaussian03 with UB3LYP/EPRII. For the rotation of the methyl groups, all relevant geometries have been considered and Boltzmann-weighted to obtain the values listed in the table.

Value / mT	0.833	-0.428	0.0868	-0.722	1.30
Type	1N	2H	2H	1H	6H

Table S3: Used hyperfine coupling constants for 9,10-dimethyl anthracene$^{\bullet-}$ taken from [9].

Value / mT	0.388	-0.290	-0.152
Type	6H	4H	4H

Table S4: Used hyperfine coupling constants for Py-h$_{10}^{\bullet-}$ taken from [10].

Value / mT	-0.475	0.109	-0.208
Type	4H	2H	4H

Table S5: Used hyperfine coupling constants for Py-d$_{10}^{\bullet-}$. The values are estimated from the values for Py$^{\bullet-}$ assuming: $\frac{a_D}{a_H} \sim \frac{g_{n,D}}{g_{n,H}} \simeq 0.15$.

Value / mT	-0.0729	0.0167	-0.0319
Type	4D	2D	4D

References

[1] Justinek, M.; Grampp, G.; Landgraf, S.; Hore, P. J.; Lukzen, N. N. Electron Self-Exchange Kinetics Determined by MARY Spectroscopy: Theory and Experiment. *J. Am. Chem. Soc.* **2004**, *126*, 5635–5646.

[2] Lukzen, N. N.; Kattnig, D. R.; Grampp, G. The effect of signs of hyperfine coupling constant on MARY spectra affected by degenerate electron exchange. *Chem. Phys. Lett.* **2005**, *413*, 118–122.

[3] Gorelik, V. R.; Bagryanskaya, E. G.; Lukzen, N. N.; Koptyug, I. V.; Perov, V. V.; Sagdeev, R. Z. Stationary and Time-Resolved Dynamic Nuclear Polarization in Weak Magnetic Fields in the Presence of Degenerate Electron Exchange. *J. Phys. Chem.* **1996**, *100*, 5800–5807.

[4] Kattnig, D. R.; Rosspeintner, A.; Grampp, G. Fully Reversible Interconversion between Locally Excited Fluorophore, Exciplex, and Radical Ion Pair Demonstrated by a New Magnetic Field Effect. *Angew. Chem., Int. Ed.* **2008**, *47*, 960–962.

[5] Rosspeintner, A.; Kattnig, D. R.; Angulo, G.; Landgraf, S.; Grampp, G. The Rehm-Weller Experiment in View of Distant Electron Transfer. *Chem. - Eur. J.* **2008**, *14*, 6213–6221.

[6] Swallen, S. F.; Weidemaier, K.; Fayer, M. D. Solvent structure and hydrodynamic effects in photoinduced electron transfer. *J. Chem. Phys.* **1996**, *104*, 2976–2986.

[7] Deutch, J.; Felderhof, B. Hydrodynamic effect in diffusion-controlled reaction. *J. Chem. Phys.* **1973**, *59*, 1669–1671.

[8] Rosspeintner, A.; Kattnig, D. R.; Angulo, G.; Landgraf, S.; Grampp, G.; Cuetos, A. On the Coherent Description of Diffusion-Influenced Fluorescence Quenching Experiments. *Chem. - Eur. J.* **2007**, *13*, 6474–6483.

[9] Bolton, J.; Carrington, A.; McLachlan, A. Electron spin resonance studies of hyperconjugation in aromatic ions. *Mol. Phys.* **1962**, *5*, 31–41.

[10] Gerson, F.; Huber, W. *Electron Spin Resonance Spectroscopy for Organic Radicals*, 1st ed.; Wiley-VCH, 2001.